ACS APPLIED NANO MATERIALS

www.acsanm.org Article

In Situ Surface-Enhanced Raman Scattering Detection of a SARS-CoV-2 Biomarker Using Flexible and Transparent Polydimethylsiloxane Films with Embedded Au Nanoplates

Weiling Yue,[†] Zhichao Xia,[†] Zhiyou Zeng, Zhinan Chen, Ling Qiao, Panjie Li,* Yi He,* and Xiaojun Luo*

Cite This: *ACS Appl. Nano Mater.* 2022, 5, 12897−12906 Read Online

ABSTRACT: Coronavirus disease 2019 (COVID-19) remains an ongoing issue worldwide and continues to disrupt daily life. Transmission of infection primarily occurs through secretions when in contact with infected individuals, but more recent evidence has shown that fomites are also a source of virus transmission, especially in cold-chain logistics. Traditional nucleic acid testing for severe acute respiratory syndrome coronavirus 2 (SARS-CoV-2) contamination in cold-chain logistics is time-consuming and inaccurate because of the multiplex sampling sites. Surface-enhanced Raman spectroscopy (SERS) provides a rapid, sensitive, and label-free detection route for various molecules, including viruses, through the identification of the characteristic peaks of their outer membrane proteins. In this study, we embedded arbitrarily orientated gold nanoplates (Au NPLs) in polydimethylsiloxane (PDMS) elastomer and used it as biosensor for the ultrasensitive detection of the SARS-CoV-2 spike protein in cold-chain logistics. This transparent and flexible substrate can be wrapped onto arbitrary surfaces and permits light penetration into the underlying contact surface, enabling in situ and point-of-care SERS diagnostics. The developed assay displayed high reproducibility (8.7%) and a low detection limit of 6.8×10^{-9} g mL^{-1}, indicating its potential to serve as a promising approach with increased accuracy and sensitivity for the detection of the S protein.

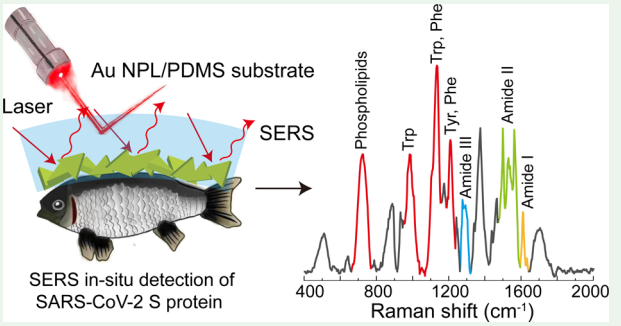

KEYWORDS: *SERS, in situ, spike protein, flexible, transparent*

INTRODUCTION

The coronavirus disease 2019 (COVID-19) outbreak caused by severe acute respiratory syndrome coronavirus 2 (SARS-CoV-2) has become a worldwide emergency and still interferes with our daily life, because RNA viruses have high infectivities, pathogenicities, and mutation rates.[1,2] It is widely accepted that the virus is transmitted by aerosols from infected individuals' saliva when talking, sneezing, or coughing.[3] Aside from aerosols in the air, direct contact with contaminated surfaces is another mode of transmission.[4] Pastorino et al. and many other groups have identified that fomite transmission, especially cold-chain products contaminated with SARS-CoV-2, acts as a vector for the transmission of SARS-CoV-2, should not be ignored.[5,6] The first reported cluster associated with cold-chain logistics was an outbreak in Beijing's Xinfadi market in June 2020. Subsequently, more local outbreaks with cases connected to cold-chain logistics were reported in Dalian, Tianjin, Shanghai, and Quanzhou in China.[7] Furthermore, researchers have demonstrated that the virus is more infectious and stable when stored at −20 °C than at room temperature.[8] Another study found that the infectivity and persistence of SARS-CoV-2 can be prolonged in a protein-rich environment, such as fish, pork, beef, or other food products.[5] This kind of "fomite-to-person" transmission in cold-chain logistics increases pathogen transmission complexity, suggesting that we should strictly monitor cold-chain food sanitation, strengthen cold-chain transmission prevention measures, and reduce the risk of novel coronavirus transmission.

As inanimate objects cannot produce antibodies, antibody testing cannot be used to identify novel coronaviruses on cold-chain surfaces. Therefore, the most widely used method for SARS-CoV-2 detection in cold-chain products is nucleic acid testing based on quantitative reverse transcription-polymerase chain reaction (qRT-PCR).[9] However, this technique requires the extraction of RNA from swab samples and time-consuming pretreatment, which normally exceeds 4 h.[10] More importantly, the contaminated areas on cold-chain surfaces or food

Received: June 24, 2022
Accepted: August 8, 2022
Published: August 19, 2022

https://doi.org/10.1021/acsanm.2c02750
ACS Appl. Nano Mater. 2022, 5, 12897−12906

packaging are randomly distributed, and additional areas should be tested to obtain accurate results. An increase in the number of sampling sites increases the cost of testing. Additionally, the complex sample collection process and environmental interference may cause false-negative results and are unsuitable for on-site detection. Therefore, increased research on the accurate and rapid detection of SARS-CoV-2 contamination in cold-chain logistics is warranted.

Testing for SARS-CoV-2 antigens is an appropriate alternative, which has already been available for the diagnosis of respiratory viruses, such as respiratory syncytial viruses, influenza, and SARS-CoV-1, and has even been urgently launched for SARS-CoV-2.[11] SARS-CoV-2 is a coronavirus type that is characterized by the presence of four structural proteins: spike (S), membrane (M), nucleocapsid (N), and envelope (E).[12] The S protein is located on the surface of the virus and is responsible for mediating attachment and entry into the host cell.[13] The S protein plays an important role in virus transmission and is one of the most valuable antigen biomarkers for virus detection, because viral proteins exist not only in living organisms but also on the surface of objects.[14] Compared to nucleic acid testing, antigen detection is relatively faster, simpler, less expensive, and is beneficial in point-of-care diagnostic methodologies.[15] Therefore, antigen detection has distinct advantages for carrying out large-scale virus screening in cold-chain logistics.

Label-free surface-enhanced Raman spectroscopy (SERS) detection has emerged as a popular candidate for antigen detection because of its capability to provide fingerprint information with ultrahigh sensitivity at the single-molecule level.[16] SERS spectrum not only contains structure information about the identities of the adsorbed analytes, but also provides their orientations on the substrate surface, providing chemically specific signals to identify the species.[17] SERS is also notable for its rapid detection speed and operational convenience.[18] No pretreatment, such as centrifugation, rupture, separation, or other complicated procedures, is required, and we can directly obtain the fingerprint information on the S protein located at the viral surface for real-time and point-of-care diagnostics. More accurate detection results can be obtained by scanning a large detection area of the cold-chain logistics surface. However, conventional SERS substrates constructed based on glass sides or silicon wafers are usually rigid and unsuitable for the direct detection of analytes adsorbed on curved surfaces, particularly for the detection molecules in fish, meat, and fruit in cold-chain logistics. Thus, there has been an increase in the focus on an effective SERS sensor with a high electromagnetic field (*E*-field) enhancement ability, transparency, and flexibility for in situ cold-chain detection.

Here, we chose polydimethylsiloxane (PDMS) as the support layer because of its nontoxicity, chemical inertness, and transparency.[19,20] In addition, its flexible ability as well as its "stickiness" were highly satisfying advantages for the targeted application in situ food monitoring, as they can be effectively swabbed onto curved surfaces.[21] A jellylike flexible substrate was developed via PDMS coupled with an oil/water interface self-assembly technique. Finally, a single-layer and arbitrarily orientated Au triangular nanoplate (Au NPL) film embedded in the PDMS layer, referred to as the Au NPL/PDMS substrate, was obtained. On the one hand, the localized surface plasmon resonance of Au triangular NPLs provides large *E*-field enhancement.[22] On the other hand, the PDMS layer provides transparency and flexibility, which is beneficial for in situ and noninvasive SERS detection.[19] Additionally, compared with other assembly methods of PDMS films based on various nanoparticles, our fabrication process is much simpler, which avoids complex surface modification and ligand exchange methods. The fabricated substrate allows plasmon interaction with the analytical surface, and hence effectively enhances SERS responses. The SERS intensity is directly related to the numbers of analytes absorbed on the Au NPL/PDMS film, which establishes the basis of the measurements. Next, we explored its applications for rapid S protein detection in cold-chain fish scales using SERS. First, for the S protein remaining on the outer skin, the fabricated Au NPL/PDMS substrate can easily be adhered to contaminated and curved fish skin because of its sticky and flexible nature. This is the least destructive method using back laser illumination for in situ SERS detection. Second, S protein can be easily extracted from fish scales through a microextraction procedure (also known as the "paste-and-peel off" method),[23] and the obtained samples can be stored and taken back to the laboratory for further SERS-based detection by front illumination. All these results indicate that our-proposed SERS platform shows great potential for the in situ and off-site monitoring of S protein residues in cold-chain logistics.

EXPERIMENTAL SECTION

Synthesis of Au Triangular NPLs. The Au triangular NPL solution (edge length = 100 ± 12 nm) was synthesized using a seed-mediated growth methodology.[24,25] First, Au spherical nanoparticle seeds with a diameter of 4 nm were prepared by the following steps. One-haf a milliliter of 10 mM aqueous chloroauric acid ($HAuCl_4 \cdot 3H_2O$) and 0.5 mL of 10 mM trisodium citrate were added into 18 mL of deionized water. Then, 0.5 mL of 100 mM freshly ice-cold sodium borohydride solution was added. The color changed from colorless to reddish orange. Stirring was stopped after 2 min and the solution was left undisturbed for 2−4 h.

To prepare Au triangular NPLs, we prepared three growth solutions as follows. The first growth solutions 1 and 2 comprised cetyltrimethylammonium bromide (CTAB, 50 mM, 9 mL), sodium hydroxide (NaOH, 100 mM, 0.05 mL), potassium iodide (KI, 10 mM, 0.05 mL), $HAuCl_4$ (10 mM, 0.25 mL), and ascorbic acid (AA, 100 mM, 0.05 mL). The growth solution 3 contained CTAB (50 mM, 90 mL), NaOH (100 mM, 0.5 mL), KI (10 mM, 0.5 mL), $HAuCl_4$ (10 mM, 2.5 mL), and ascorbic acid (100 mM, 0.5 mL). Au triangular NPLs were initiated by adding 1 mL of Au seeds into growth solution 1. Then, 1 mL of the mixed solution was added into growth solution 2. After 5 s of shaking, the whole solution 2 was poured into growth solution 3 and stored at 30 °C. After 1 day, the precipitation was carefully collected at the bottom of the reaction vessel and the supernatant was removed by three rounds of centrifugation (4000 rpm, 10 min).

Self-Assembly of Au Triangular NPL Film and Au NPL-Embedded PDMS Substrate. Premade purified Au triangular NPL colloid (6 mL) was added to a glass container, followed by the addition of 2 mL of hexane to form a water/hexane interface. Subsequently, 1−2 mL of ethanol was slowly added to the mixture. After the evaporation of hexane and ethanol, a large, mirror-like metallic sheen area floating on the water surface was observed, which showed successful self-assembly of the Au triangular NPL film. Thereafter, a freshly piranha-cleaned silicon (10 mm × 10 mm) was carefully slid beneath the Au triangular NPL film and slowly lifted from the water. After air drying, the film-covered silicon was immersed in 1% toluene solution of octadecyltrimethoxysilane (OTS) at 60 °C for 2 days, followed by gently washing with acetone, DI water at 25 °C for 10 s, and drying with N_2 stream.

Subsequently, a mixture of PDMS (the ratio of Slygard 184 base and curing agent is 10:1) was poured onto the OTS-treated silicon

https://doi.org/10.1021/acsanm.2c02750
ACS Appl. Nano Mater. 2022, 5, 12897−12906

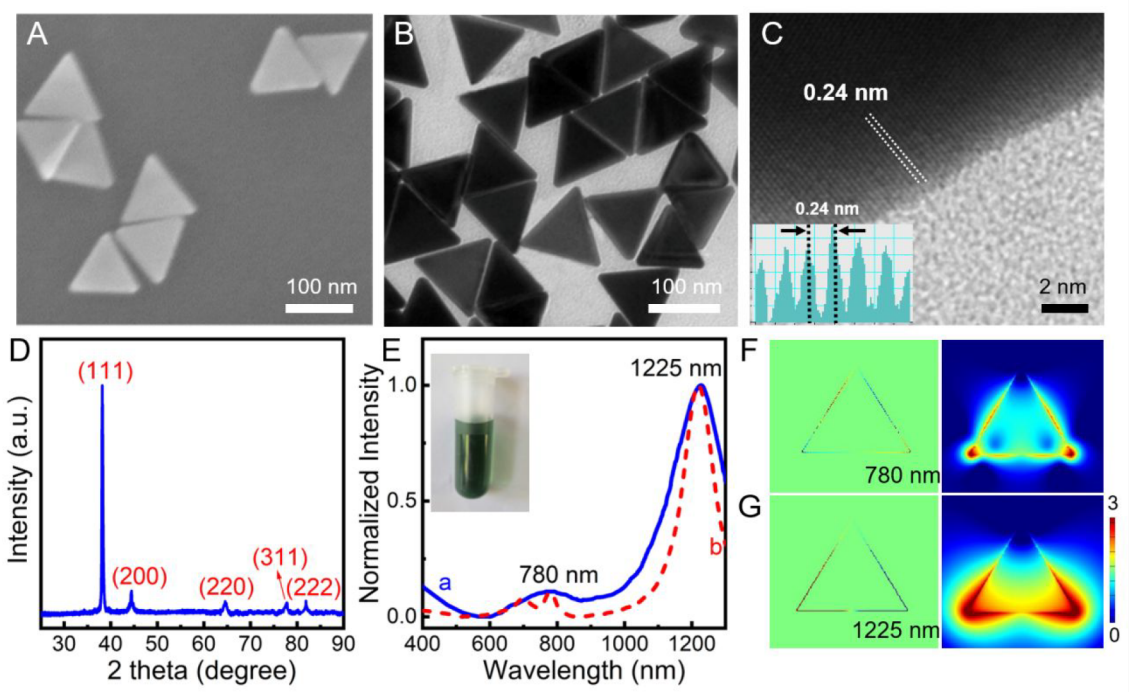

Figure 1. (A) SEM image, (B) TEM image, (C) HRTEM image, and (D) XRD pattern of the as-synthesized Au triangular NPLs. The inset in C is the inverse fast Fourier transformation (FFT) patterns of the Au NPL colloid. (E) Experimental (a) and FDTD-simulated (b) extinction spectra for the Au NPLs (the colors of the colloids shown in the inset). (F and G) Charge distributions (left) and corresponding *E*-field distribution profiles (right) for a single Au triangular NPL at wavelengths of 780 and 1225 nm, respectively. The scale bar represents $(E_{max}/E_0)^2$ on a log scale.

surface and allowed to stand for 1 h at 25 °C to release air bubbles in the PDMS. Next, the PDMS-coated substrate was heat at 70 °C for 10 h to solidify the PDMS. After natural cooling, the Au NPL/PDMS can be easily peeled from the silicon master. Finally, the Au triangular NPL film was completely transferred into PDMS.

SERS Measurements. Raman and SERS measurements were obtained from a Labram HR 800 microspectrometer (Jobin Yvon) equipped with a 785 nm laser with a 0.5 mW power. The laser spot is ~1 μm in radius. All spectra (range of 400 cm^{-1} to 2000 cm^{-1}) were smoothed and baselined using LabSpec 5 software. The collection time of each SERS spectrum was set as 10 s, and each spectrum was accumulated five times.

Raman reporter rhodamine 6G (Rh6G) was used to investigate the SERS activity of the preprepared Au NPLs. Rh6G (100 μL, 1 nM) was deposited onto the substrate and left to evaporate at 25 °C for 30 min. SERS signals were directly collected by both front and back illumination of the Au NPL/PDMS substrate. Reproducibility data were acquired by collecting the SERS responses from 30 different sites on the Au NPL/PDMS substrate surface randomly. Mechanical capabilities assessments were carried out by measuring the Rh6G solution before and after bending, torsion, and stretching of the substrate for 100 cycles. For S protein sensitivity measurements, 100 μL of aqueous S protein solutions of different concentrations (1×10^{-9} to 1×10^{-4} g mL^{-1}) were deposited onto clean Au NPL/PDMS at 25 °C for 30 min. The measurements were collected using back-illumination. For real sample detection, 100 μL of aqueous S protein solution was dropped onto dried fish skin for 30 min for backside SERS measurement. S protein microextraction was performed by pressing the top surface of Au NPL/PDMS substrate against the S protein-contaminated fish scales for 2 min and then removing it. The SERS measurements were subsequently performed on the front side of the SERS substrate.

■ RESULTS AND DISCUSSION

Fabrication and Characterization of Au Triangular NPLs. A seed-mediated synthesis strategy was used to fabricate triangular Au NPLs in three growth solutions.[24,25] As shown in Figure 1A, B, the edge length of the as-synthesized Au triangular NPLs was measured to be 100 ± 12 nm. Compared with nanostars and nanobranches, the large surface areas and flat morphologies of Au NPLs provided open and easily accessible surface topologies for biomolecules to access and adsorb.[24] The Fringe spacing and diffractions pattern of the Au NPLs was around 0.24 nm, which is close to the spacing of bulk Au {111} (0.236 nm), confirming that the {111} surface was exposed on the top surface (Figure 1C). In addition, the XRD pattern in Figure 1D confirms that the Au NPLs were grown along the (111) direction with the help of iodide ions. The inset in Figure 1E shows that the color of the purified Au NPL suspension was dark green. The experimentally measured and simulated extinction spectra of Au NPLs were collected and shown in Figure 1E. Two LSPR peaks were observed in the measured spectrum, among which the first peak had wavelength-matched surface plasmons with the desired laser wavelength. Thus, we can use 785 nm laser source to excite resonance Raman scattering, because excitation via a near-infrared (NIR) laser helps minimize the autofluorescence background of biomolecules, which is more suitable for the biological window. The second peak was located at 1225 nm and appeared broader than the simulated spectrum. This was caused by random orientations, and several prisms with irregularly shaped existed in the Au NPL colloid. As depicted in Figure 1F, G, the corresponding charge contours of the Au triangular NPLs at the two plasmonic peaks were attributed to quadrupole and dipole resonances. Additionally, strong local *E*-field distributions were confined to the sharp vertices and side edges of the Au NPLs, indicating high SERS enhancement ability of the Au NPLs, which is higher than some traditional nanospheres, nanorods, nanocubes, and on par with some

https://doi.org/10.1021/acsanm.2c02750
ACS Appl. Nano Mater. 2022, 5, 12897−12906

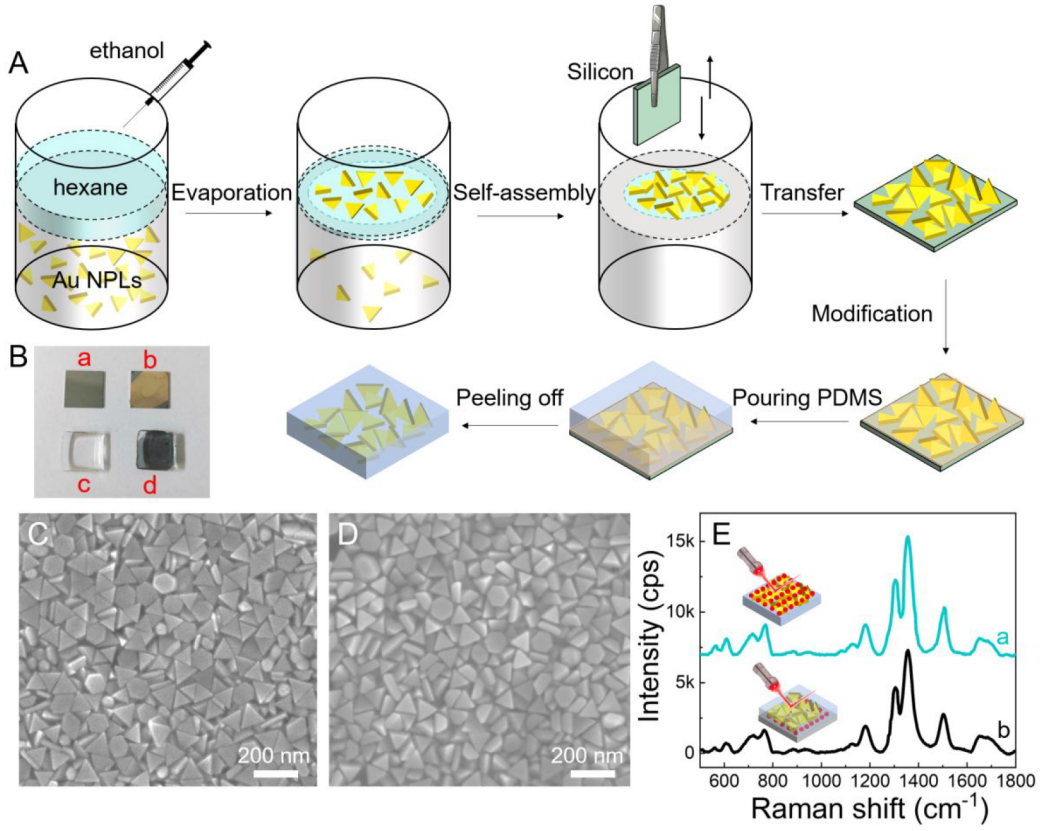

Figure 2. (A) Schematic illustration of the as-proposed fabrication process of Au NPL/PDMS SERS substrate. (B) Photograph of (a) bare silicon, (b) Au NPL film on silicon, (c) bare PDMS, and (d) Au NPL film-embedded PDMS. (C) SEM image of self-assembled Au NPL film on a silicon substrate. (D) SEM image of the self-assembled Au NPL film embedded into PDMS. (E) SERS spectra of 1 nM Rh6G collected from both sides of the Au NPL/PDMS substrate.

nanostructures with spikey protrusions.[26] It should also be noted that a shorter wavelength appeared at 700 nm in the theoretical extinction spectra, which is ascribed to the octupolar plasmon mode (the corresponding charge contour is shown in Figure S1). However, it is difficult to observe this mode in experiments because of the inhomogeneous size distribution and the huge difficulty in sustaining high-order plasmon mode.[24,26]

Fabrication and Characterization of a Flexible Au NPL/PDMS Substrate. Motivated by the high *E*-field distribution and rich resonance modes of Au NPLs, we deposited Au NPLs on different substrates to avoid their aggregation of Au NPLs in solution during detection. Because of efficient and convenient oil/water interface self-assembly technology, the assembled monolayer film can be equipped with superior uniformity and controllability, which is beneficial in improving SERS performance. Figure 2A shows the fabrication process of the large-area distributed SERS substrate. Self-assembled Au triangular NPL film were first transferred from the hexane/water interface onto a rigid substrate (e.g., silicon wafer) and then onto the flexible PDMS polymer film. Briefly, hexane was carefully added to the Au NPL colloid to form a hexane/water interface between the two immiscible liquids. Then, 1−2 mL of ethanol was dropped slowly, causing the Au NPLs to be driven from water to the interface and formed a large-area Au NPL film. After the evaporation of hexane and ethanol, we transferred this close-packed film onto a piranha-cleaned silicon substrate using the Langmuir−Blodgett transfer technique.[27,28] As shown in Figure 2B, a mirrorlike metallic sheen was generated across the entire substrate after the Au NPL film was transferred onto a bare silicon wafer. Because silicon wafers are rigid and opaque, PDMS was selected as the support layer because of its chemical inertness, nontoxicity, and transparency. Next, the unoccupied silicon area uncovered by Au NPL film was passivated by adding OTS solution.[29] After passivation, the PDMS precursor was poured onto its surface. Finally, the Au NPL/PDMS substrate was easily removed from the silicon wafer. The Au NPL film on silicon was successfully transferred to the PDMS polymer, which subsequently changed color, as seen in Figure 2B. The size of our fabricated Au NPL/PDMS substrate was 10 mm × 10 mm, and the average thickness of the free-standing substrate was measured to be ∼2 mm (Figure S2). We can also increase the size of Au NPL/PDMS substrate to expand the detection range of large analytes. SEM images of the Au NPL film assembled on silicon and transferred onto the PDMS film are displayed in Figure 2C, D. One cannot avoid generating a small number of hexagonal Au NPLs, spherical particles, and prisms with irregular shapes during the synthesis of Au triangular NPLs; however, the yield of triangular Au NPLs was still estimated to be 80−100%. We found that the Au NPL film formed on silicon and PDMS substrate was close-packed but randomly oriented because no surface modification or ligand exchange was involved in the experiment. The majority of Au NPLs tended to lie horizontally, whereas a small number of Au NPLs were vertically or arbitrarily arranged. Previous studies have demonstrated that these vertically aligned Au NPLs show higher SERS enhancements than

https://doi.org/10.1021/acsanm.2c02750
ACS Appl. Nano Mater. 2022, 5, 12897−12906

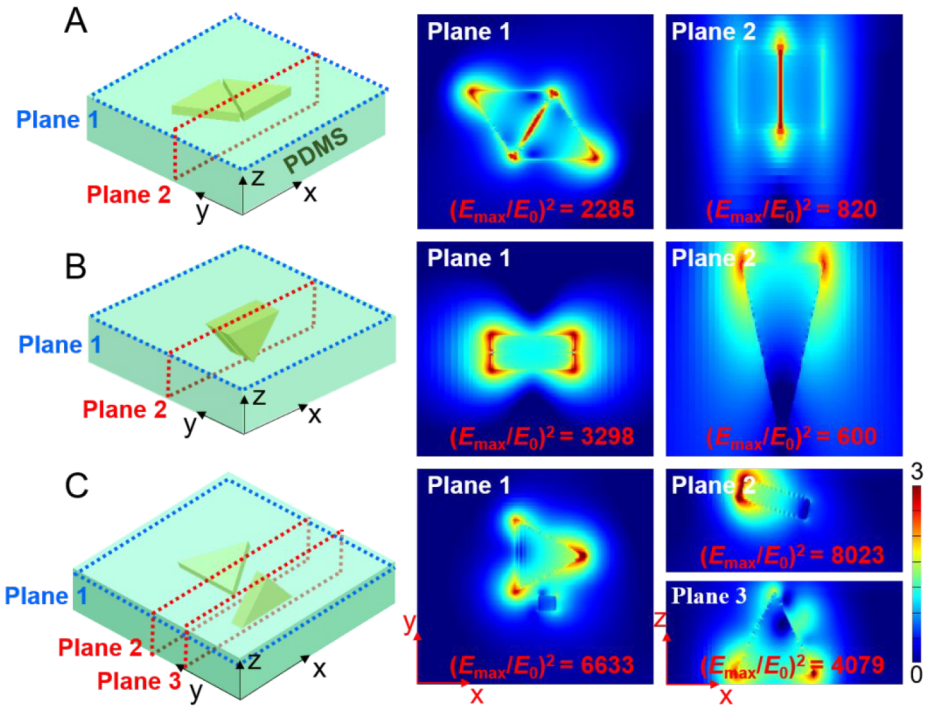

Figure 3. Sketch of structure layouts and corresponding *E*-field distributions at different planes of Au NPLs on PDMS substrate for FDTD simulations under a 785 nm laser: (A) horizontal-to-horizontal model, (B) vertical-to-vertical model, and (C) horizontal-to-vertical model. The scale bar represents $(E_{max}/E_0)^2$ on a log scale.

horizontal ones. Additionally, the vertical aligned Au NPLs are more favorable for analyte molecules to approach than horizontal Au NPLs due to probable steric and electrostatic charge effect of the substrate surface.[30,31] Moreover, plasmonic coupling between adjacent and randomly orientated Au NPLs generated small nanogaps and altered the plasmonic properties. This small interparticle distance formed a high density of "hot spots", thus significantly boosting the intensity of the SERS signals of the analytes adsorbed on its surface.

The SERS spectra of 1 nM Rh6G were collected to assess the SERS enhancement ability of the Au NPL/PDMS substrate. Because PDMS possesses excellent optical transparency, the laser can easily pass through the PDMS polymer and reach the assembled Au NPL film. SERS signals were collected from both sides and compared, as shown in Figure 2E. Curve a: 1 nM Rh6G was directly dropped onto substrate with Au NPL film on the top side and recorded SERS spectra. Curve b: 1 nM Rh6G was dropped onto the same frontside, while SERS spectra was recorded upon backside laser irradiation. The SERS signal intensity upon backside laser irradiation was almost identical to that upon irradiation from the frontside, and both SERS spectra were significantly enhanced from either the front or back side of the Au NPL/PDMS substrates, compared to the normal Raman spectrum of Rh6G (1.0 mM) depicted in Figure S3. It was believed that PDMS shows a weak Raman signal and gives a rather "clean" SERS background even though it was close to Au NPLs. Hence, the SERS signal collected directly from the backside of the PDMS would not be sacrificed when the substrate was wrapped over the object's surface. Several characteristic peaks, C−H out of-plane bending (765 cm^{-1}), C−H in-plane bending (1180 cm^{-1}), N−H in-plane bending (1302 cm^{-1}), and C−C stretching vibration modes (1354 and 1505 cm^{-1}), were observed and enhanced in the spectra[32,33] according to the following equation: AEF $\approx \frac{I_{SERS}/C_{SERS}}{I_{RS}/C_{RS}}$, where I_{SERS} and I_{RS} represent the SERS and normal Raman intensities. C_{SERS} and C_{RS} are the concentration of Rh6G molecules detected in SERS and Raman measurement.[34,35] The analytical enhancement factor (AEF) of our as-fabricated Au NPL/PDMS can reach ~6.3 × 10^7 when detected from the frontside, and ~5.8 × 10^7 when detected from the backside. The high enhancement of our fabricated Au NPL/PDMS substrate is more superior than most of the previous reported plasmon materials/PDMS substrates because of its high density of "hot spots" and easily accessible surface topology, resulting in highly sensitive detection of target molecules (Table S1). Moreover, even though the Au NPLs were randomly oriented on PDMS substrate, the average "hot spot" densities within the laser focal spot (~1 μm in radius) were uniform in different detection sites. Thus, the spectra obtained at different spots were highly reproducible (Figure S4), due to the average effect. The relative standard deviation (RSD) value of the peak intensity at 1354 cm^{-1} from back illumination was 8.7%, which is lower than that of a commercial Klarite substrate (~10%).[32] With the help of hexane/water self-assembly technology, Langmuir−Blodgett transfer technique, flexibility and transparency of PDMS, our fabricated Au NPL/PDMS substrates yielded strong and highly reproducible signals. Therefore, the proposed method is a great potential candidate for in situ practical applications.

FDTD Simulations of Au NPL/PDMS Substrate. FDTD simulations were performed to assess and understand the *E*-field distribution of the Au NPL/PDMS substrate. A closer look at the SEM images in Figure 2D suggests three main assembly patterns of Au NPLs, i.e., horizontal-to-horizontal, vertical-to-vertical, and horizontal-to-vertical. Thus, we built three simplified arrangements of Au NPLs on the top PDMS for FDTD simulations (Figure 3). In the first model, two Au

https://doi.org/10.1021/acsanm.2c02750
ACS Appl. Nano Mater. 2022, 5, 12897−12906

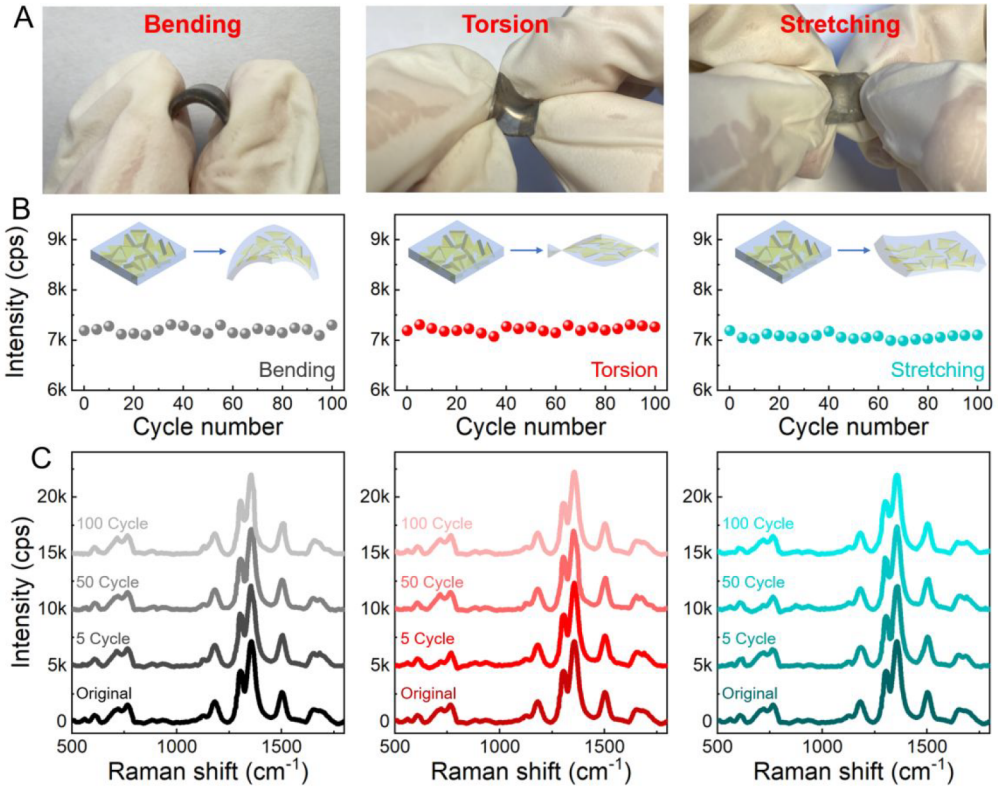

Figure 4. (A) Photograph of the flexible characteristics of Au NPL/PDMS substrate including the bending, torsion, and stretching. (B, C) Corresponding SERS intensity at 1354 cm^{-1} and SERS spectra after bending, torsion, and stretching for 100 cycles.

NPLs stood side-by-side and parallel to the PDMS substrate; we defined it as a horizontal-to-horizontal model. The second model was two Au NPLs aligned face-to-face and perpendicular to the substrate (denoted as the vertical-to-vertical model). The third model had one Au NPL nearly parallel and another Au NPL perpendicular to the PDMS substrate (termed as horizontal-to-vertical model). The FDTD-simulated *E*-field distribution and intensity for the three models in different planes under 785 nm plane-wave excitation are shown in Figure 3. The "hot spot" was confined around the vertexes of each Au NPL as well as in the gap between adjacent Au NPLs. The enhancement factor (E_F) for SERS is roughly proportional to $(E_{max}/E_0)^4$.[36] It shows a maximum *E*-field intensity $(E_{max}/E_0)^2$ of ~6.6×10^3 of the horizontal-to-vertical model at $x-y$ plane (plane 1). $(E_{max}/E_0)^2$ was found to be more intense a the t $x-z$ plane (~8.0×10^3, plane 2) and less intense at plane 3 (~4.1×10^3). In general, the enhancement ability of the horizontal-to-vertical model was much more intense than that of horizontal-to-horizontal and vertical-to-vertical models in both the $x-y$ and $x-z$ planes. For better comparison, we set up several other control groups in Figure S5, and we found that the average *E*-field intensities of randomly oriented Au NPLs on PDMS substrate were stronger than orderly arranged ones. In addition, when we simulated more Au NPLs in FDTD simulations (Figure S6), the same results can be obtained. Thus, these simulation results demonstrated that we did not have to fabricate well-ordered standing or lying Au NPL arrays on solid substrates through complex surface modification and ligand exchange methods, and the formation of randomly oriented and disorganized Au NPLs on the PDMS substrate was conducive to generating stronger *E*-field enhancement. As a result, the calculation results provided probative information for us to compare the SERS performances of differently oriented Au NPLs, and we found that our fabricated, randomly oriented Au NPLs on PDMS was an optimal choice for SERS applications, while maintaining the reproducibility of the results.

Mechanical Capabilities of the Au NPL/PDMS Substrate. In addition to the strong and highly reproducible SERS performance of the flexible SERS substrate, the Au NPL/PDMS substrate also displayed excellent mechanical stability. This means that it was flexible enough to withstand bending, twisting, and stretching without breaking, making it useful in practical applications.[37] Figure 4A–C shows the photographs of the Au NPL/PDMS substrate on bending, torsion, and stretching status in the naked eyes. For the bending and torsion tests, the flexible SERS substrate was bent in half and twisted at 180° for 100 cycles. For the stretching tests, the Au NPL/PDMS substrate was 1.5× elongated for 100 cycles. No detectable changes were observed in the SERS spectra when the Au NPL/PDMS substrate was restored to the original state. In addition, their SERS intensity maintained a similar value at the peak of 1354 cm^{-1} compared to the original state before the mechanical stimuli. The above results indicate that the Au NPL/PDMS substrates exhibit good flexibility and mechanical robustness, which are beneficial for substrates in close contact with target analytes on curved or nonplanar surfaces in practical applications. In this way, in situ SERS detection can be analyzed by simply coating target analytes with Au NPL/PDMS film and using backside illumination.

Sensing Capabilities of Transparent and Flexible Au NPL/PDMS Substrate. Motivated by its high SERS performance, we further explored the Au NPL/PDMS as a sensing platform to detect the SARS-CoV-2 biomarker. There is

https://doi.org/10.1021/acsanm.2c02750
ACS Appl. Nano Mater. 2022, 5, 12897−12906

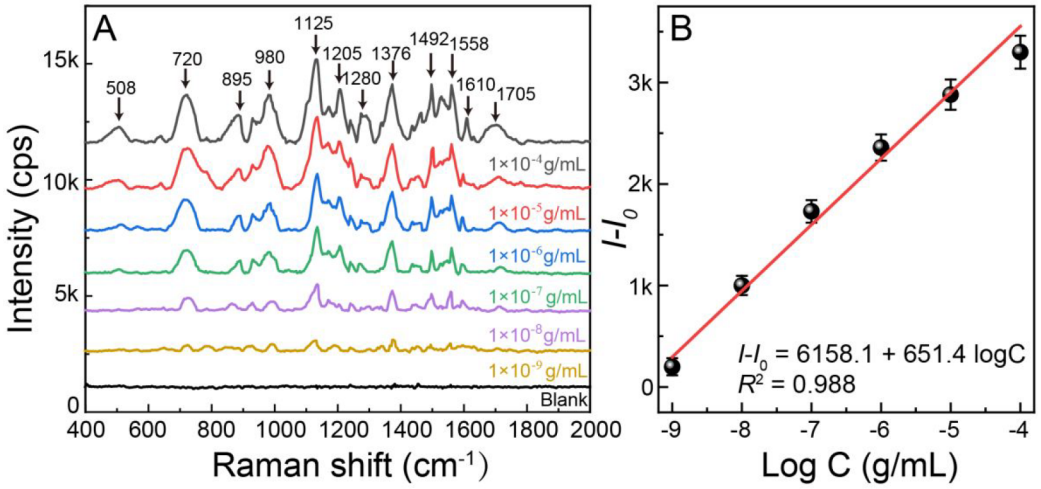

Figure 5. (A) Averaged SERS spectra of the SARS-CoV-2 S protein at different concentrations ranging from 1×10^{-9} to 1×10^{-4} g mL^{-1} collected on Au NPL/PDMS substrate through backside laser irradiation. (B) Dependence of the SERS intensity at 1125 cm^{-1} on the S protein concentrations on a logarithmic scale, the error bar was obtained from five independent experiments. I_0 and I represent the SERS intensity of Au NPL/PDMS substrate before and after absorbing the S protein, respectively.

agreement that SERS is a near-field effect and the *E*-field enhancement would quickly diminish within ~10 nm from the sensing surface.[38] Therefore, SERS is able to analyze only the composition of the surface of a virus and is hardly to detect the whole virus molecular information through label-free SERS detection. S protein is the outer membrane protein of the virus, and the size is within the *E*-field enhancement region.[13] Thus, we chose the S protein as the detection object. The obtained SERS spectra were measured for a series of diluted S protein aqueous solutions from 1×10^{-9} to 1×10^{-4} g mL^{-1} in Figure 5A. All spectra were collected using backside laser irradiation and averaged over five independent experiments. For the excitation wavelength, integration times and laser power used, no typical PDMS Raman peaks were found in our study. Numerous bands can be distinctly recognized to obtain structure information on the S protein even at low concentrations, including some secondary structure Raman bands at 1280 cm^{-1} (amide III), 1492−1592 cm^{-1} (amide II), and 1610 cm^{-1} (amide I).[39,40] Additionally, some typical Raman bands attributed to amino acid side-chains were also well discerned, including tryptophan (Trp) bands at 980 and 1125 cm^{-1}, tyrosine (Tyr) band at 1205 cm^{-1}, phenylalanine (Phe) bands at 1125 and 1205 cm^{-1}, and CH_2 bending band of proteins at 1705 cm^{-1}. Detailed assignments of the Raman bands are shown in Table S2, and these bands are consistent with the previous report.[41−43] However, these well-defined Raman peaks were indistinctly observed when the concentration was decreased to 1×10^{-10} M and 1×10^{-9} g mL^{-1}. A linearity relationship established between the SERS intensity at 1125 cm^{-1} and the logarithm of the target S protein concentration, that is $I - I_0 = 6158.1 + 651.4 \log C$ with a high correlation coefficient (R^2) of 0.988 (Figure 5B). The LOD of the assay was determined to be 6.8×10^{-9} g mL^{-1}, which was calculated via the International Union of Pure and Applied Chemistry (IUPAC) standard method ($Y_L = Y_B + 3SD$, where Y_B is the average SERS intensity of the blank sample and 3SD represent three times of the standard deviation of the blank sample signal).[44] The detailed calculation was shown in the Supporting Information. The linear range was from 1×10^{-9} to 1×10^{-4} g mL^{-1}, indicating the broad detection range and good sensitivity of the Au NPL/PDMS platform. Even though the LOD of our assay was much higher than indirect SERS detection due to the smaller scattering cross section of protein molecules than Raman reporter molecules.[45] Notably, the LOD of this assay was 1×10^4 times more sensitive than other label-free SERS method owing to the much stronger *E*-field enhancement of the randomly arranged Au NPLs on PDMS substrate.[46] What's more, our sensitivity was lower than some field-effect transistor and electrical impedance spectroscopy sensors listed in Table S3, but our method was notable for its rapid detection speed (~30 min) and operational convenience.

SARS-CoV-2 residues in cold-chain foods have become a serious risk to human health. To evaluate practical applications of the Au NPL/PDMS substrate, we carried out an S protein test on fish scales from cold-chain storage using the developed substrate. First, 1×10^{-8} g mL^{-1} of S protein was dropped onto a small area (diameter ~1 cm) of fish scale and then air-dried for 30 min. Then, we attached the flexible Au NPL/PDMS substrate directly onto the preprepared S protein-contaminated fish skin, followed by SERS back illumination. Each SERS spectrum from the Au NPL/PDMS substrate was randomly collected and an average from five spectra from different sampling sites was obtained. Because of the good flexibility and transparency of the Au NPL/PDMS substrate, the in situ SERS signal of the S protein could be successfully detected from the contaminated fish scale (curve a). Further, due to the "sticky" nature of PDMS polymer, detection by microextraction was then demonstrated, which provided an alternative method of identification of S protein in fish scale.[21,23] Specifically, the Au NPL/PDMS substrates were placed and pressed on the fish scales with Au NPLs side facing the skin and in contact with the analytical surface for 2 min for microextraction. In this process, S proteins can spontaneously form a self-assembled monolayer on the Au NPL surface quickly aided by several forces such as hydrogen bonds, solvation forces, van der Waals interactions, etc.[47] Then, the S protein absorbed Au NPL/PDMS was peeled off, followed by front SERS illumination. The SERS spectra of the S protein were recorded within 2 min. The SERS spectra recorded on the microextracted S protein are illustrated in curve b of Figure 6, and the intensity of the spectrum was comparable to those

https://doi.org/10.1021/acsanm.2c02750
ACS Appl. Nano Mater. 2022, 5, 12897−12906

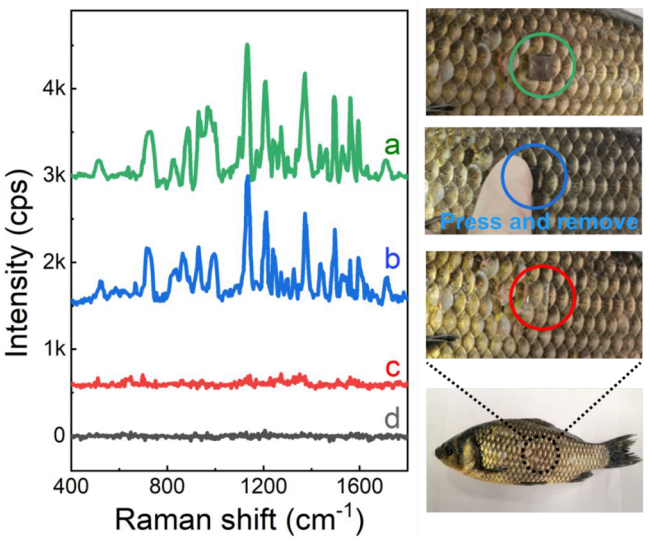

Figure 6. SERS spectra and corresponding photograph of (a) fish scale loaded with S protein (1×10^{-8} g mL^{-1}) and coated with Au NPL/PDMS substrate, and then illuminated from the backside with a 785 nm laser; (b) S protein obtained from microextracted method and illuminating from the frontside; (c) fish scale coated with PDMS only (without S protein); (d) fish scale loaded with 1×10^{-4} g mL^{-1} S protein only (without substrate). Each spectrum was averaged from five spectra at different sampling sites.

obtained by direct back illumination. In contrary, there were no evident SERS signals from the uncontaminated fish scales covered with only PDMS polymer (curve c). In addition, there were no signals when a laser directly illuminated the fish scale with the S protein molecule, without the SERS substrate (curve d). This method provides two SARS-CoV-2 residues detection methods, both in situ and off-site. The overall time of in situ and off-site detection in our system was around 30 min, which is faster than traditional qRT-PCR-based nucleic acid detection,[9] endowing it a promising candidate for the fast detection of targets from real environments. Our detection method is also expected to be extended to other applications, such as the detection of residual pesticides on fruit or vegetable surfaces.

Despite the advantages and convenience SERS technology may offer, there are still challenges being faced in the process of developing the technique. The specificity is important in analysis methods. In general, Raman spectra of different proteins always exhibit many overlapping peaks because they share many same intrinsic chemical bonds. However, due to "fingerprint" identification ability of SERS, characteristic peaks of different proteins of virus can still be captured by SERS. For example, Sanchez and co-workers have demonstrated that the SERS spectroscopy of SARS-CoV-2 S and N proteins can be easily identified because of the spectral difference.[48] Thus, SERS could distinguish S proteins from other proteins, making specificity possible. Another issue that needs to be addressed is that in actual applications, cold-chain samples does not contain only the SARS-CoV-2 virus, there could be other viruses and biochemicals present in the sample. Thus, it is difficult to analysis the SERS spectra due to the interferences brought by these unwanted chemicals to some degree. Principal component analysis (PCA), multivariate curve resolution (MCR), and linear discriminant analysis (LDA) are appropriate tools for analyzing complex SERS data as well as in clinical diagnosis.[49−51] These statistical analysis methods generate score and loading plots that can maximize the differences of the similar spectral data, and can be further utilized to discriminate SARS-CoV-2 S protein spiked positive and negative samples in complex system. The combination of SERS with statistical methods may provide a precise and sensitive diagnosis method of S protein, as well as other proteins in complex system.

CONCLUSIONS

In summary, we have fabricated a flexible and transparent SERS sensor as a simple and rapid SERS-based technique for highly sensitive and accurate SERS detection of the S protein on fish scales by embedding a randomly orientated Au NPL film into the PDMS layer. Compared with well-ordered standing or lying Au NPL film on PDMS, disorganized Au NPLs on the PDMS substrate is more conducive to generating stronger *E*-field enhancement through FDTD simulations. The Au NPL/PDMS substrate exhibited a high SERS enhancement when detected from front and back sides, and it also exhibited good signal reproducibility, with an RSD value of 8.7%. Together with the excellent mechanical stability, flexibility, and transparency of PDMS, the Au NPL/PDMS substrate was further used to detect the SARS-CoV-2 biomarker, S protein. The developed assay displays ultrasensitivity with a broad linear range (1×10^{-9} to 1×10^{-4} g mL^{-1}) and a low detection limit (6.8×10^{-9} g mL^{-1}). Finally, this sensor was used to monitor SARS-CoV-2 residues on fish scales in cold-chain storage. The proof of concept for the in situ analytical application of the SERS substrate was provided through the direct SERS detection of the S protein on the fish surface, and the results indicated that the Au NPL/PDMS substrate had great potential for the in situ ultrasensitive detection of S protein residues on irregular objects. The entire analysis protocol in this work is simple, noninvasive, and fast (the measurement takes ∼30 min to complete). Therefore, our fabricated substrate provided new insights for developing more stable and portable sensors for both in situ and off-site detection of target molecules in the future, especially in food safety and environmental monitoring.

ASSOCIATED CONTENT

Supporting Information

The Supporting Information is available free of charge at https://pubs.acs.org/doi/10.1021/acsanm.2c02750.

Materials, Instrument, FDTD simulations, calculation of LOD, Comparison of the performance of different PDMS substrates, Raman bands of typical vibrational modes of the S protein, Comparison of the performance of different techniques for the S protein, FDTD simulated charge distribution contour of Au NPLs, normal Raman spectrum of Rh6G, SERS spectra of 30 independent assays, and different FDTD simulated structures of Au NPs/PDMS substrates (PDF)

AUTHOR INFORMATION

Corresponding Authors

Panjie Li − *School of Chemistry and Chemical Engineering, School of Environmental and Biological Engineering, Nanjing University of Science and Technology, Nanjing 210094, China*; Email: lpjchemical@163.com

https://doi.org/10.1021/acsanm.2c02750
ACS Appl. Nano Mater. 2022, 5, 12897−12906

Yi He − *School of Science, Xihua University, Chengdu 610039, P. R. China*; Email: heyi@mail.xhu.edu.cn
Xiaojun Luo − *School of Science, Xihua University, Chengdu 610039, P. R. China*; orcid.org/0000-0002-3899-0105; Email: xajunluo@hotmail.com

Authors

Weiling Yue − *School of Science, Xihua University, Chengdu 610039, P. R. China*
Zhichao Xia − *School of Science, Xihua University, Chengdu 610039, P. R. China*
Zhiyou Zeng − *School of Science, Xihua University, Chengdu 610039, P. R. China*
Zhinan Chen − *School of Science, Xihua University, Chengdu 610039, P. R. China*
Ling Qiao − *Division of Chemistry and Biological Chemistry, School of Physical & Mathematical Sciences, Nanyang Technological University, Singapore 637371, Singapore*

Complete contact information is available at: https://pubs.acs.org/10.1021/acsanm.2c02750

Author Contributions

†W.Y. and Z.X. contributed equally to this work.

Notes

The authors declare no competing financial interest.

■ ACKNOWLEDGMENTS

We greatly appreciate the financial support from PhD Scientific Research Startup Foundation of Xihua University (RZ2100002826) and the Postgraduate Research & Practice Innovation Program of Jiangsu Province (KYCX21-0354). L.Q. thanks the China Scholarship Council (CSC) for its support (202006860052).

■ REFERENCES

(1) Syed, A. M.; Taha, T. Y.; Tabata, T.; Chen, I. P.; Ciling, A.; Khalid, M. M.; Sreekumar, B.; Chen, P.-Y.; Hayashi, J. M.; Soczek, K. M.; Ott, M.; Doudna, J. A. Rapid Assessment of SARS-CoV-2 Evolved Variants Using Virus-Like Particles. *Science* **2021**, *374*, 1626−1632.
(2) Wise, J. Covid-19: the E484K Mutation and the Risks it Poses. *BMJ.* **2021**, n359.
(3) Liu, J.; Li, Y.; Liu, L.; Hu, X.; Wang, X.; Hu, H.; Hu, Z.; Zhou, Y.; Wang, M. Infection of Human Sweat Glands by SARS-CoV-2. *Cell Discovery* **2020**, *6*, 84.
(4) Van Doremalen, N.; Bushmaker, T.; Morris, D. H.; Holbrook, M. G.; Gamble, A.; Williamson, B. N.; Tamin, A.; Harcourt, J. L.; Thornburg, N. J.; Gerber, S. I.; Lloyd-Smith, J. O.; de Wit, E.; Munster, V. J. Aerosol and Surface Stability of SARS-CoV-2 as Compared with SARS-CoV-1. *N. Engl. J. Med.* **2020**, *382*, 1564−1567.
(5) Pastorino, B.; Touret, F.; Gilles, M.; de Lamballerie, X.; Charrel, R. N. Prolonged Infectivity of SARS-CoV-2 in Fomites. *Emerging Infect. Dis* **2020**, *26*, 2256−2257.
(6) Ji, W.; Li, X.; Chen, S.; Ren, L. Transmission of SARS-CoV-2 Via Fomite, Especially Cold Chain, Should Not be Ignored. *Proc. Natl. Acad. Sci. U. S. A* **2021**, *118*, No. e2026093118.
(7) Li, Y.; Liu, H.; Xia, W.; Wong, G. W. K.; Xu, S. Cold Chain Logistics: A Possible Mode of SARS-CoV-2 Transmission? *BMJ.* **2021**, *375*, No. e066129.
(8) Chin, A. W. H.; Chu, J. T. S.; Perera, M. R. A.; Hui, K. P. Y.; Yen, H. L.; Chan, M. C. W.; Peiris, M.; Poon, L. L. M. Stability of SARS-CoV-2 in Different Environmental Conditions. *Lancet Microbe* **2020**, *1*, No. E10.
(9) Corman, V. M.; Landt, O.; Kaiser, M.; Molenkamp, R.; Meijer, A.; Chu, D. K.; Bleicker, T.; Brünink, S.; Schneider, J.; Schmidt, M. L.; et al. Detection of 2019 Novel Coronavirus (2019-nCoV) by Real-Time RT-PCR. *Eurosurveillance* **2020**, *25*, 23−30.
(10) Zhang, Z.; Wang, H.; Su, M.; Sun, Y.; Tan, S.-J.; Ponkratova, E.; Zhao, M.; Wu, D.; Wang, K.; Pan, Q.; Chen, B.; Zuev, D.; Song, Y. Printed Nanochain-Based Colorimetric Assay for Quantitative Virus Detection. *Angew. Chem., Int. Ed* **2021**, *60*, 24234−24240.
(11) Carter, L. J.; Garner, L. V.; Smoot, J. W.; Li, Y.; Zhou, Q.; Saveson, C. J.; Sasso, J. M.; Gregg, A. C.; Soares, D. J.; Beskid, T. R.; Jervey, S. R.; Liu, C. Assay Techniques and Test Development for COVID-19 Diagnosis. *ACS Cent. Sci.* **2020**, *6*, 591−605.
(12) Li, F. Structure, Function, and Evolution of Coronavirus Spike Proteins. *Annu. Rev. Virol* **2016**, *3*, 237−261.
(13) Nguyen, N. H. L.; Kim, S.; Lindemann, G.; Berry, V. COVID-19 Spike Protein Induced Phononic Modification in Antibody-Coupled Graphene for Viral Detection Application. *ACS Nano* **2021**, *15*, 11743−11752.
(14) Kalantar-Zadeh, K.; Ward, S. A.; Kalantar-Zadeh, K.; El-Omar, E. M. Considering the Effects of Microbiome and Diet on SARS-CoV-2 Infection: Nanotechnology Roles. *ACS Nano* **2020**, *14*, 9202−9202.
(15) Babiker, A.; Myers, C. M.; Hill, C. E.; Guarner, J. SARS-CoV-2 Testing. *Am. J. Clin. Pathol* **2020**, *153*, 706−708.
(16) Kneipp, K.; Wang, Y.; Kneipp, H.; Perelman, L. T.; Itzkan, I.; Dasari, R.; Feld, M. S. Single Molecule Detection Using Surface-Enhanced Raman Scattering (SERS). *Phys. Rev. Lett.* **1997**, *78*, 1667−1670.
(17) Li, J.-F.; Zhang, Y.-J.; Ding, S.-Y.; Panneerselvam, R.; Tian, Z.-Q. Core-Shell Nanoparticle-Enhanced Raman Spectroscopy. *Chem. Rev.* **2017**, *117*, 5002−5069.
(18) Zong, C.; Xu, M.; Xu, L.-J.; Wei, T.; Ma, X.; Zheng, X.-S.; Hu, R.; Ren, B. Surface-Enhanced Raman Spectroscopy for Bioanalysis: Reliability and Challenges. *Chem. Rev.* **2018**, *118*, 4946−4980.
(19) Ma, Y.; Du, Y.; Chen, Y.; Gu, C.; Jiang, T.; Wei, G.; Zhou, J. Intrinsic Raman Signal of Polymer Matrix Induced Quantitative Multiphase SERS Analysis Based on Stretched PDMS Film with Anchored Ag Nanoparticles/Au Nanowires. *Chem. Eng. J.* **2020**, *381*, 122710.
(20) Fortuni, B.; Inose, T.; Uezono, S.; Toyouchi, S.; Umemoto, K.; Sekine, S.; Fujita, Y.; Ricci, M.; Lu, G.; Masuhara, A.; Hutchison, J. A.; Latterini, L.; Uji-i, H. In Situ Synthesis of Au-shelled Ag Nanoparticles on PDMS for Flexible, Long-life, and Broad Spectrum-Sensitive SERS Substrates. *Chem. Commun.* **2017**, *53*, 11298−11301.
(21) Alyami, A.; Quinn, A. J.; Iacopino, D. Flexible and Transparent Surface Enhanced Raman Scattering (SERS)-Active Ag NPs/PDMS Composites for In-situ Detection of Food Contaminants. *Talanta* **2019**, *201*, 58−64.
(22) Zhou, L.; Zhou, J.; Lai, W.; Yang, X.; Meng, J.; Su, L.; Gu, C.; Jiang, T.; Pun, E. Y. B.; Shao, L.; et al. Irreversible Accumulated SERS Behavior of the Molecule-Linked Silver and Silver-Doped Titanium Dioxide Hybrid System. *Nat. Commun.* **2020**, *11*, 1785.
(23) Jiang, J.; Zou, S.; Ma, L.; Wang, S.; Liao, J.; Zhang, Z. Surface-Enhanced Raman Scattering Detection of Pesticide Residues Using Transparent Adhesive Tapes and Coated Silver Nanorods. *ACS Appl. Mater. Interfaces* **2018**, *10*, 9129−9135.
(24) Qin, F.; Zhao, T.; Jiang, R.; Jiang, N.; Ruan, Q.; Wang, J.; Sun, L.-D.; Yan, C.-H.; Lin, H.-Q. Thickness Control Produces Gold Nanoplates with Their Plasmon in the Visible and Near-Infrared Regions. *Adv. Opt. Mater.* **2016**, *4*, 76−85.
(25) Hong, S.; Shuford, K. L.; Park, S. Shape Transformation of Gold Nanoplates and Their Surface Plasmon Characterization: Triangular to Hexagonal Nanoplates. *Chem. Mater.* **2011**, *23*, 2011−2013.
(26) Luo, X.; Qiao, L.; Xia, Z.; Yu, J.; Wang, X.; Huang, J.; Shu, C.; Wu, C.; He, Y. Shape- and Size-Dependent Refractive Index Sensing and SERS Performance of Gold Nanoplates. *Langmuir* **2022**, *38*, 6454−6463.
(27) Tao, A.; Kim, F.; Hess, C.; Goldberger, J.; He, R.; Sun, Y.; Xia, Y.; Yang, P. Langmuir-Blodgett Silver Nanowire Monolayers for Molecular Sensing Using Surface-Enhanced Raman Spectroscopy. *Nano Lett.* **2003**, *3*, 1229−1233.

(28) Kim, F.; Kwan, S.; Akana, J.; Yang, P. Langmuir-Blodgett Nanorod Assembly. *J. Am. Chem. Soc.* **2001**, *123*, 4360−4361.
(29) Lu, G.; Li, H.; Zhang, H. Gold-Nanoparticle-Embedded Polydimethylsiloxane Elastomers for Highly Sensitive Raman Detection. *Small* **2012**, *8*, 1336−1340.
(30) Yin, H.; Guo, Y.; Cui, X.; Lu, W.; Yang, Z.; Yang, B.; Wang, J. Plasmonic and Sensing Properties of Vertically Oriented Hexagonal Gold Nanoplates. *Nanoscale* **2018**, *10*, 15058−15070.
(31) Tian, X.-D.; Lin, Y.; Dong, J.-C.; Zhang, Y.-J.; Wu, S.-R.; Liu, S.-Y; Zhang, Y.; Li, J.-F.; Tian, Z.-Q. Synthesis of Ag Nanorods with Highly Tunable Plasmonics Toward Optimal Surface-Enhanced Raman Scattering Substrates Self-Assembled at Interfaces. *Adv. Opt. Mater.* **2017**, *5*, 1700581.
(32) Luo, X.; Xing, Y.; Galvan, D. D.; Zheng, E.; Wu, P.; Cai, C.; Yu, Q. Plasmonic Gold Nanohole Array for Surface-Enhanced Raman Scattering Detection of DNA Methylation. *ACS Sens* **2019**, *4*, 1534−1542.
(33) Luo, X.; Jiang, L.; Kang, T.; Xing, Y.; Zheng, E.; Wu, P.; Cai, C.; Yu, Q. Label-Free Raman Observation of TET1 Protein-Mediated Epigenetic Alterations in DNA. *Anal. Chem.* **2019**, *91*, 7304−7312.
(34) Tran, V.; Thiel, C.; Svejda, J. T.; Jalali, M.; Walkenfort, B.; Erni, D.; Schlücker, S. Probing the SERS Brightness of Individual Au Nanoparticles, Hollow Au/Ag Nanoshells, Au Nanostars and Au Core/Au Satellite Particles: Single-Particle Experiments and Computer Simulations. *Nanoscale* **2018**, *10*, 21721−21731.
(35) Jin, M.; Pully, V.; Otto, C.; Van den Berg, A.; Carlen, E. T. High-Density Periodic Arrays of Self-Aligned Subwavelength Nanopyramids for Surface-Enhanced Raman Spectroscopy. *J. Phys. Chem. C* **2010**, *114*, 21953−21959.
(36) Lin, L.; Zhang, Q.; Li, X.; Qiu, M.; Jiang, X.; Jin, W.; Gu, H.; Lei, D. Y.; Ye, J. Electron Transport Across Plasmonic Molecular Nanogaps Interrogated with Surface-Enhanced Raman Scattering. *ACS Nano* **2018**, *12*, 6492−6503.
(37) Park, S.; Lee, J.; Ko, H. Transparent and Flexible Surface-Enhanced Raman Scattering (SERS) Sensors Based on Gold Nanostar Arrays Embedded in Silicon Rubber Film. *ACS Appl. Mater. Interfaces* **2017**, *9*, 44088−44095.
(38) Pilot, R.; Signorini, R.; Durante, C.; Orian, L.; Bhamidipati, M.; Fabris, L. A Review on Surface-Enhanced Raman Scattering. *Biosensors* **2019**, *9*, 57.
(39) Stanborough, T.; Given, F. M.; Koch, B.; Sheen, C. R.; Stowers-Hull, A. B.; Waterland, M. R.; Crittenden, D. L. Optical Detection of CoV-SARS-2 Viral Proteins to Sub-Picomolar Concentrations. *ACS Omega* **2021**, *6*, 6404−6413.
(40) Daoudi, K.; Ramachandran, K.; Alawadhi, H.; Boukherroub, R.; Dogheche, E.; El Khakani, M. A.; Gaidi, M. Ultra-Sensitive and Fast Optical Detection of the Spike Protein of the SARS-CoV-2 Using AgNPs/SiNWs Nanohybrid Based Sensors. *Surf. Interfaces* **2021**, *27*, 101454.
(41) Kahraman, M.; Sur, I.; Culha, M. Label-Free Detection of Proteins from Self-Assembled Protein-Silver Nanoparticle Structures Using Surface-Enhanced Raman Scattering. *Anal. Chem.* **2010**, *82*, 7596−7602.
(42) Hernández-Arteaga, A. C.; Ojeda-Galván, H. J.; Rodríguez-Aranda, M. C.; Toro-Vázquez, J. F.; Sánchez, F.; José-Yacamán, M.; Navarro-Contreras, H. R. Determination of the Denaturation Temperature of the Spike protein S1 of SARS-CoV-2 (2019 nCoV) by Raman Spectroscopy. *Spectrochim. Acta, Part A* **2022**, *264*, 120269.
(43) Bangaru, S.; Ozorowski, G.; Turner, H. L.; Antanasijevic, A.; Huang, D.; Wang, X.; Torres, J. L.; Diedrich, J. K.; Tian, J.-H.; Portnoff, A. D.; et al. Structural Analysis of Full-Length SARS-CoV-2 Spike Protein from an Advanced Vaccine Candidate. *Science* **2020**, *370*, 1089−1094.
(44) *Compendium of Chemical Terminology, Gold Book, Version 2.3.3*; International Union of Pure and Applied Chemistry, 2014; Vol. *528*.
(45) Zhang, M.; Li, X.; Pan, J.; Zhang, Y.; Zhang, L.; Wang, C.; Yan, X.; Liu, X.; Lu, G. Ultrasensitive Detection of SARS-CoV-2 Spike Protein in Untreated Saliva Using SERS-Based Biosensor. *Biosens. Bioelectron.* **2021**, *190*, 113421.
(46) Payne, T. D.; Klawa, S. J.; Jian, T.; Kim, S. H.; Papanikolas, M. J.; Freeman, R.; Schultz, Z. D. Catching COVID: Engineering Peptide-Modified Surface-Enhanced Raman Spectroscopy Sensors for SARS-CoV-2. *ACS Sens.* **2021**, *6*, 3436−3444.
(47) Saptarshi, S. R.; Duschl, A.; Lopata, A. L. Interaction of Nanoparticles with Proteins: Relation to Bio-Reactivity of the Nanoparticle. *J. Nanobiotechnol* **2013**, *11*, 26.
(48) Sanchez, J. E.; Jaramillo, S. A.; Settles, E.; Velazquez Salazar, J. J.; Lehr, A.; Gonzalez, J.; Rodriguez Aranda, C.; Navarro-Contreras, H. R.; Raniere, M. O.; Harvey, M.; et al. Detection of SARS-CoV-2 and Its S and N Proteins Using Surface Enhanced Raman Spectroscopy. *RSC Adv.* **2021**, *11*, 25788−25794.
(49) Lim, J.-Y.; Nam, J.-S.; Shin, H.; Park, J.; Song, H.-I.; Kang, M.; Lim, K.-I.; Choi, Y. Identification of Newly Emerging Influenza Viruses by Detecting the Virally Infected Cells Based on Surface Enhanced Raman Spectroscopy and Principal Component Analysis. *Anal. Chem.* **2019**, *91*, 5677−5684.
(50) Payne, T. D.; Klawa, S. J.; Jian, T.; Kim, S. H.; Papanikolas, M. J.; Freeman, R.; Schultz, Z. D. Catching COVID: Engineering Peptide-Modified Surface-Enhanced Raman Spectroscopy Sensors for SARS-CoV-2. *ACS Sens.* **2021**, *6*, 3436−3444.
(51) Zhang, D.; Zhang, X.; Ma, R.; Deng, S.; Wang, X.; Wang, X.; Zhang, X.; Huang, X.; Liu, Y.; Li, G.; Qu, J.; Zhu, Y.; Li, J. Ultra-Fast and Onsite Interrogation of Severe Acute Respiratory Syndrome Coronavirus 2 (SARS-CoV-2) in Waters via Surface Enhanced Raman Scattering (SERS). *Water Res.* **2021**, *200*, 117243.

https://doi.org/10.1021/acsanm.2c02750
ACS Appl. Nano Mater. 2022, 5, 12897−12906